

# Corn Seedling Monitoring Using 3-D Point Cloud Data From Terrestrial Laser Scanning and Registered Camera Data

Lijun Xu<sup>ID</sup>, Senior Member, IEEE, Teng Xu, and Xiaolu Li<sup>ID</sup>, Member, IEEE

**Abstract**—In precision farming, the separation of crops from soil is crucial for monitoring growth and fertilization. In this letter, a novel method is proposed for the accurate detection of corn seedlings from cropland by combining terrestrial laser scanning (TLS) and camera data. First, a piecewise linear interpolation method was used to eliminate the effect of distance on the TLS intensity data for more accurate intensity features of scanned targets. Second, the point cloud and camera data were registered to obtain the true color of each point in the point cloud. Third, we used a random forest algorithm to separate corn seedlings from soil by combining the geometric features from the TLS data with the radiometric features including the corrected intensity and RGB values derived from the TLS and camera data. To evaluate the proposed method, a case study was conducted by using a commercial TLS sensor with an embedded camera. The results demonstrated that corn seedlings can be separated from soil with an accuracy of 98.8% by using both the geometric and radiometric features, which is significantly higher than that by using any one of the two kinds of features.

**Index Terms**—Classification accuracy, corn seedling detection, intensity correction, precision farming, terrestrial laser scanning (TLS).

## I. INTRODUCTION

CROP growth parameters, such as crop height, crop emergence, and biomass, are all important for agricultural production management [1], [2]. These growth parameters can be used to monitor crop growth and optimize fertilizer in precision farming. To determine these growth parameters, the crop should be detected and separated from the farmland soil. Therefore, crop detection is crucial for the monitor of crop growth and fertilization in precision farming.

Some passive optical sensors, such as infrared, multispectral, and RGB cameras, have been used to extract crop properties, employing radiometric information like RGB values in precision farming [3]–[5]. These optical sensors

Manuscript received October 13, 2018; revised February 8, 2019 and April 24, 2019; accepted May 6, 2019. Date of publication May 31, 2019; date of current version December 27, 2019. This work was supported in part by the National Natural Science Foundation of China under Grant 61671038 and Grant 61721091 and in part by the Program for Changjiang Scholars and Innovative Research Team in University under Grant IRT16R02. (Corresponding author: Xiaolu Li.)

L. Xu and X. Li are with the Beijing Advanced Innovation Center for Big Data-Based Precision Medicine, Beijing 100191, China, and also with the State Key Laboratory of Inertial Science and Technology, School of Instrument Science and Opto-Electronic Engineering, Beihang University, Beijing 100191, China (e-mail: lijunxu@buaa.edu.cn; xiaoluli@buaa.edu.cn).

T. Xu is with the State Key Laboratory of Inertial Science and Technology, School of Instrument Science and Opto-Electronic Engineering, Beihang University, Beijing 100191, China (e-mail: xu\_teng@126.com).

Color versions of one or more of the figures in this letter are available online at <http://ieeexplore.ieee.org>.

Digital Object Identifier 10.1109/LGRS.2019.2916348

can provide 2-D distribution of crops for site-specific crop management. However, crops and weeds with approximate RGB values are not efficiently separated only by using radiometric information. Furthermore, sundry objects in a farmland are often mixed or overlapped in 2-D images and have a negative effect on the crop detection [6]. Light detection and ranging (LiDAR), as an active remote sensing technique, has an advantage over passive remote sensing in its ability to obtain 3-D geometric information of crops [7], [8]. In particular, terrestrial laser scanning (TLS) can provide more accurate and higher point density data about 3-D geometric information of crops. In addition to 3-D measurements for geometrical information ( $X$ ,  $Y$ ,  $Z$ ) of crops, TLS can also record radiometric information about scanned crops including intensity data and RGB values captured by a digital camera integrated with LiDAR [9]. Radiometric information derived from TLS data has been also applied to crop detection, nitrogen prediction, and separation of foliar and woody materials [10]–[12]. Although radiometric and geometric information derived from TLS data have been used separately, their joint use has the potential to greatly improve the classification accuracy of crops and soil. Therefore, the combination of geometric and radiometric information for separation of crop and soil requires to be further explored.

However, TLS raw intensity data are influenced by some factors such as the system transmission, atmosphere, distance, incident angle, and physical characteristics of scanned surfaces [13]–[15]. For raw intensity data obtained by the same TLS sensor at one project, the system transmission effect on TLS intensity data can be considered as a constant and the atmospheric effect can be ignored for short-range TLS. Therefore, distance and incident angle effects on TLS intensity data should be eliminated so that corrected intensity of TLS is related only to the physical characteristics of scanned crops. The corrected intensity data as a radiometric feature can be applied to the separation of crops and soil in precision farming.

The aim of this letter is to accurately detect crop seedling by using TLS data and camera data. To improve the separability of corn seedlings and other classes (soil, weeds, etc.), both geometric and radiometric features derived from TLS data and camera data are applied in the random forest algorithm. The remainder of this letter is organized as follows. The method of crop detection is introduced in Section II. Study area and data acquisition are presented in Section III. Experimental results and discussion are described in Section IV. Section V summarizes the conclusions of this letter.

## II. METHODS

### A. Intensity Correction of TLS Data

Due to some factors that include the brightness reduction [16] and receiver's defocusing [17] at near distance, the recorded intensity of many TLS sensors commonly displays a complex intensity-distance relationship, rather than satisfying a LiDAR equation. Furthermore, distance effect functions for different types of TLS sensors usually differ from each other, and the common function of distance effect is obtained with difficulty for different types of TLS sensors. However, the intensity-distance relationship can be considered as an approximately linear function within a small distance. Thus, the distance effect on TLS intensity data can be eliminated by using a piecewise linear interpolation method in this letter, which is suitable for different types of TLS sensors.

A reference target with the reflectance of  $\rho_s$  is scanned by a TLS sensor under a fixed incidence angle of  $\theta_s$  at a series of distances  $R_i$  ( $R_i < R_{i+1}$ ,  $i = 1, 2, \dots, n - 1$ ). Meanwhile, the intensity data  $I_{dB}(R_i, \theta_s, \rho_s)$  are recorded by the TLS sensor, which is regarded as the reference intensity.

In this letter, a TLS sensor (model: RIEGL VZ-400i) was used to obtain TLS data of scanned objects, and the returned intensity of scanned objects can be expressed as [15], [18]

$$I_{dB}(R_x, \theta_s, \rho_s) = F_1(R_x) + F_2(\theta_s) + F_3(\rho_s) \quad (1)$$

where  $I_{dB}(R_x, \theta_s, \rho_s)$  is the recorded intensity of the reference target at the distance of  $R_x$ .  $F_1(R_x)$ ,  $F_2(\theta_s)$ , and  $F_3(\rho_s)$  are the distance effect function, the incident angle effect function, and the reflectance effect function, respectively.

The intensity value  $I_{dB}(R_x, \theta_s, \rho_s)$  can also be obtained by means of a piecewise linear interpolation as

$$I_{dB}(R_x, \theta_s, \rho_s) = \frac{I_{dB}(R_{i+1}, \theta_s, \rho_s) - I_{dB}(R_i, \theta_s, \rho_s)}{R_{i+1} - R_i} (R_x - R_i) + I_{dB}(R_i, \theta_s, \rho_s). \quad (2)$$

where the distance  $R_x$  meets the relationship  $R_i < R_x < R_{i+1}$ . Substituting (2) into (1), the following is obtained:

$$F_1(R_x) = I_{dB}(R_i, \theta_s, \rho_s) - F_2(\theta_s) - F_3(\rho_s) + \frac{I_{dB}(R_{i+1}, \theta_s, \rho_s) - I_{dB}(R_i, \theta_s, \rho_s)}{R_{i+1} - R_i} (R_x - R_i). \quad (3)$$

Assume that the recorded intensity of a scanned object with the reflectance of  $\rho$  at the distance of  $R_x$  and the incident angle of  $\theta_x$  is denoted as  $I_{dB}(R_x, \theta_x, \rho)$ . Therefore, the distance corrected intensity  $I_c(R_x, \theta_x, \rho)$  can be expressed as follows:

$$\begin{aligned} I_c(R_x, \theta_x, \rho) &= I_{dB}(R_x, \theta_x, \rho) - F_1(R_x) \\ &= I_{dB}(R_x, \theta_s, \rho_s) - \{I_{dB}(R_i, \theta_s, \rho_s) - F_2(\theta_s) - F_3(\rho_s) \\ &\quad + \frac{I_{dB}(R_{i+1}, \theta_s, \rho_s) - I_{dB}(R_i, \theta_s, \rho_s)}{R_{i+1} - R_i} * (R_x - R_i)\}. \end{aligned} \quad (4)$$

From (4), we know that the distance corrected intensity  $I_c(R_x, \theta_x, \rho)$  is related only to the incident angle effect and the reflectance of scanned targets. Because the scanned targets are small and irregular, it is difficult to estimate the incident angle,

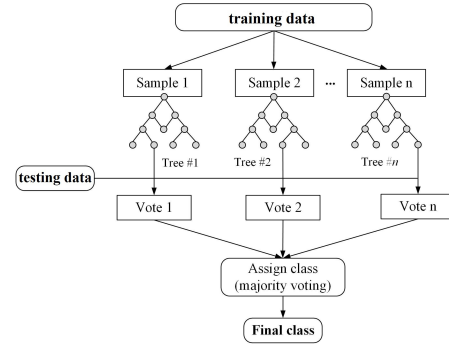


Fig. 1. Schematic of random forest algorithm.

and the incident angle effect is quite complicated. Therefore, the incident angle effect is suppressed only by using the mean intensity value in this letter. To calculate the mean intensity value, some points in the neighbor of a seed point are selected, where the diameter of the neighbor is 5 cm and there are more than 20 points in the neighbor.

### B. Data Registration

During the TLS, a TLS sensor with an embedded camera was used to obtain point cloud data and image data. To realize the fusion of 3-D point cloud and image data, it is necessary to execute the space registration of point cloud and image. Their space registration is achieved by calculating the mathematic projection relation between the image pixel coordinate and the 3-D coordinate of the point cloud. As the embedded camera was calibrated, the mathematic projection relation can be obtained to complete the space registration of point cloud and image. All the acquired data were preprocessed and registered using the RiSCAN PRO software, where the accuracy of registration is directly related to the selected features for registration and can reach up to several millimeters.

### C. Corn Seedling Detection

The random forest algorithm, an ensemble machine learning method proposed by Breiman [19], was employed in this letter, and it has become popular within the remote sensing community because of the accuracy of its classifications [20]. Compared to other machine learning methods such as the support vector machine and artificial neural network methods, there are fewer parameters to be specified when running the random forest algorithm [21]. Moreover, it is also fast and insensitive to overfitting when dealing with high dimensional data [20], [22]. The classifier of the random forest algorithm can make predictions and has been extensively exploited in forest applications using hyperspectral and LiDAR data.

To train the classification model of the random forest algorithm, some train samples were manually selected from the point cloud data and labeled as corn seedlings and others (about 500 points per class), respectively. The final results of the classifier were determined based on the output of all the trees using the majority voting. To achieve relatively higher accuracy and simultaneously reduce the amount of calculation, the number of trees was set at 50 in this letter. The schematic of the random forest algorithm is illustrated in Fig. 1.

TABLE I  
LIST OF RADIOMETRIC AND GEOMETRIC FEATURES

Radiometric features	Geometric features
Corrected intensity ( $I_c$ )	Height values
Mean of corrected intensity ( $I_m$ )	Mean of Height values
Std. of corrected intensity ( $I_{c\_Std}$ )	Std. of Height values
(R, G, B) data from camera (RGB)	

The validation for classification results was performed as follows. First, 500 points per class were randomly selected from the classification results. Second, these points were visually identified into the two classes (the corn seedling and others) so that the classification performance could be quantitatively evaluated. Finally, the classification performance of the proposed method was assessed by calculating the classification accuracy in this letter. All the geometric and radiometric features were used as inputs for the classifier of the random forest model, which are listed in Table I.

#### D. Seedling Emergence Percentage

After separating corn seedlings from the soil, individual corn seedlings were extracted based on octree. The total number of corn seedlings was then counted to calculate the emergence percentage, a key indicator to evaluate the germination of corn seeds. The emergence percentage can be expressed as follows:

$$\eta = \frac{n_{\text{emerged}}}{n_{\text{seeds}}} * 100\% \quad (5)$$

where  $n_{\text{emerged}}$  and  $n_{\text{seeds}}$  are the number of total emerged seedlings and seeds sown. The number of seeds sown can be obtained beforehand assuming that the seeds were sown uniformly in the cropland.

### III. STUDY AREA AND DATA SETS

To eliminate the distance effect on TLS raw intensity data, a calibration experiment was carried out first. In the calibration experiment, a reference target, reflectance of 30% (at 1550 nm), was scanned by using a TLS sensor RIEGL VZ-400i at different distances. The TLS sensor utilized in this letter has a near-infrared (1550 nm) laser beam with the divergence of 0.35 mrad and a range accuracy of 5 mm (one sigma at 100 m) [23].

All the scans were collected by the TLS sensor under the condition that the incident angle of the reference target was constant during data acquisition. The data acquisition for the calibration experiment was performed with the 1-m interval from 5 to 40 m. At each distance, the intensity data of laser points around the center of the reference target were obtained, and the means of the intensity data were used to eliminate the distance effect.

To detect corn seedlings, a cornfield at Haidian District, Beijing, China was scanned by using the same TLS sensor RIEGL VZ-400i. Before corn seedling detection, the acquired data including point cloud and camera data were preprocessed and registered using the RiSCAN PRO software. Then,



Fig. 2. Point cloud visualization of the corn field colored with RGB values.

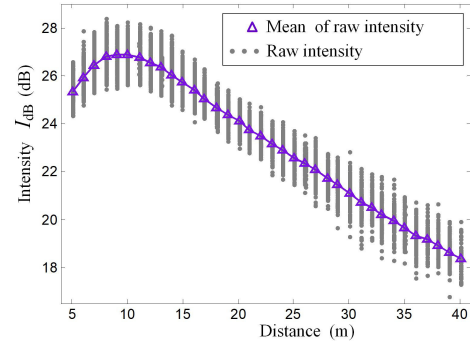


Fig. 3. Variation of raw intensity data with distance for the reference target with 30% reflectance.

TLS data from the cornfield were exported, including 3-D coordinate values, raw intensity, and RGB values of each point. Fig. 2 demonstrates the point cloud visualization of the cornfield, which is visually apparent with the true color of camera images.

## IV. RESULTS AND DISCUSSION

#### A. Intensity-Corrected TLS Data

Results of the calibration experiment are illustrated in Fig. 3. The distance effect on raw intensity data of RIEGL VZ-400i deviates from the radar range equation. However, an approximately linear relationship exists in a small distance section. Therefore, the distance effect can be eliminated by using the linear interpolation method in this letter.

LiDAR raw intensity images of a cornfield scanned with the RIEGL VZ400i are illustrated in Fig. 4(a). Due to the distance effect on raw intensity data, the raw intensity of soil changed greatly. Thus, a piecewise linear interpolation method was used to perform the intensity correction on the distance effect for the raw intensity image. The corrected intensity image, after intensity correction, is shown in Fig. 4(b). By comparing the corrected and raw intensity images, it can be seen that the distance effect has been eliminated effectively.

In the red boxes of Fig. 4, three parts were selected to statistically analyze the distributions of raw and corrected intensity data, as shown in Fig. 5. The comparison showed that the distribution of corrected intensity data was more concentrated than that of the raw intensity data, and the standard deviation of intensity data was reduced from 0.77 dB (raw intensity) to 0.55 dB (corrected intensity). Thus, after the intensity correction, the intensity value of the same object was closer, and the difference in the intensity for different objects became larger. In other words, corn seedlings and soil spots were easily distinguished in the corrected intensity image, so as to achieve the detection of corn seedlings.

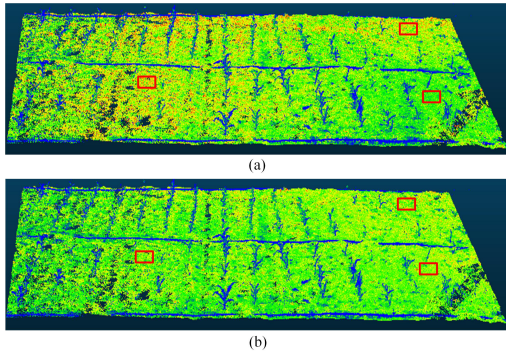


Fig. 4. LiDAR intensity images of a corn field. (a) Raw intensity image. (b) Corrected intensity image.

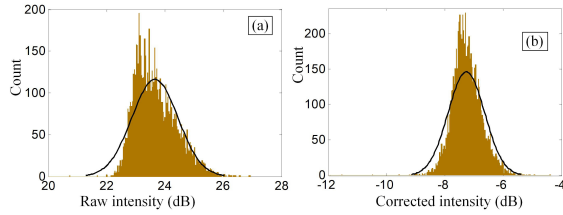


Fig. 5. (a) Histogram of raw intensity data. (b) Histogram of corrected intensity data.

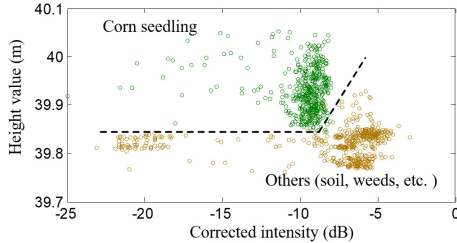


Fig. 6. Distribution of corrected intensity and height values of point clouds for corn seedlings and others.

### B. Corn Seedling Detection

The separability of corrected intensity and height values between the corn seedling and the other classes (soil, weeds, etc.) is illustrated in Fig. 6. A clear division can be seen between the corn seedling and other classes. Although some corn seedlings have lower height values, the separability of the corn seedling and other classes is not so obvious. By combining with the corrected intensity feature, the corn seedling was more effectively separated from the other classes.

As previously mentioned, the corn seedling and other classes were well separated by the joint use of geometric and radiometric features in the random forest algorithm. The classification results using geometric features, radiometric features, and their joint use in the random forest algorithm are all illustrated in Fig. 7. From the classification results, it can be seen that classification performance using the combination of geometric and radiometric features was more effective than that using either of them alone. Corn seedlings were easily separated from the soil due to their geometric features [as shown in Fig. 7(a)]. However, some parts of other classes were misclassified as the corn seedling [as shown in the red box of Fig. 7(a)] when only geometric features were used. Due to the different spectral characteristics of corn seedlings

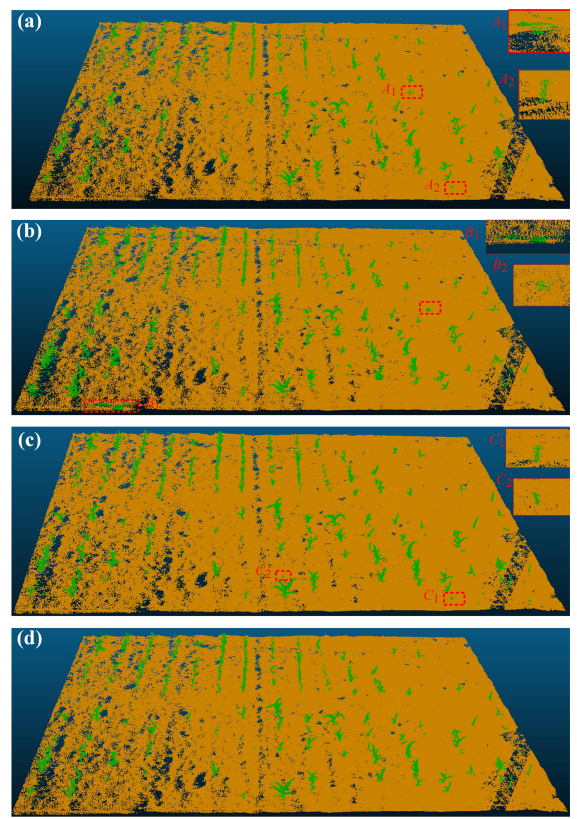


Fig. 7. Classification results (green points represent corn seedlings) using the random forest algorithm based on (a) geometric features, (b) radiometric features, (c) combination of geometric and radiometric (only corrected intensity) features, and (d) combination of geometric and radiometric (corrected intensity and RGB) features.

TABLE II  
COMPARISON OF CLASSIFICATION ACCURACIES FOR CORN SEEDLING DETECTION USING DIFFERENT FEATURES

Used features	Accuracy
Geometric	89.8%
Radiometric	82.8%
Geometric + Radiometric ( <i>only I<sub>c</sub></i> )	96.4%
Geometric + Radiometric ( <i>I<sub>c</sub> + RGB</i> )	98.8%

and soil at near-infrared band, and because some energy emitted from TLS was absorbed by crop water, corn seedlings commonly had lower intensity than that of soil and were easily separated from soil [as shown in Fig. 7(b)]. However, some targets such as weeds had smaller intensity value, similar to corn seedlings. Thus, some parts of other classes, like weeds, were also misclassified as the corn seedling [as shown in the red box of Fig. 7(b)] when using radiometric features. Fig. 7(c) and (d) illustrates that the classification performance using both radiometric and geometric features was superior to that using only one of them. Compared with the classification results shown in Fig. 7(c) and (d), the features of RGB values reduced the misclassification of crop stubble with lower intensity.

To quantitatively evaluate the classification results of corn seedlings, the classification performance using different features are listed in Table II. Detection accuracy for corn



Fig. 8. Extraction result of individual corn seedlings in Fig. 7(d) (random colors).

seedlings using geometric features or radiometric features alone was 89.8% and 82.8%. However, the detection accuracy reached 96.4% when using the combination of geometric and radiometric (only intensity) features. After RGB values were added into the radiometric features, the classification performance was improved to 98.8%, further demonstrating that classification performance for corn seedlings using the combination of radiometric and geometric features was significantly higher than that using either of them alone.

### C. Seedling Emergence Percentage

Furthermore, the individual corn seedlings shown in Fig. 7(c) were extracted based on octree in CloudCompare software [24], the extraction result of which is shown in Fig. 8. A total of 223 corn seedlings were extracted by counting the total number of individual corn seedlings. Since the seeds were uniformly sown in the cropland, the number of seeds sown can be calculated as 512. Therefore, the emergence percentage of corn seeds could be given as  $223/512 * 100\% = 43.6\%$ . The value of the emergence percentage was low, indicating the need to optimize the fertilizer and irrigation, even reseed in this area of cropland.

## V. CONCLUSION

In this letter, a novel method was proposed to accurately detect corn seedlings from the cropland by combining the geometric and radiometric features derived from TLS and camera data. Case study results indicated the following.

- 1) The intensity correction method using a piecewise linear interpolation effectively eliminated the distance effect on the TLS intensity data. Corn seedling and bare soil were more easily separated by using the intensity-corrected data.
- 2) By combining geometric and radiometric features, corn seedlings were effectively extracted from the cropland, with an accuracy of 98.8%. The classification accuracy using both of the two kinds of features was significantly higher than that using only one of them.
- 3) After RGB values were added to the radiometric features, the misclassification of crop stubbles with lower intensity values was eliminated, further improving the classification accuracy.

## ACKNOWLEDGMENT

The authors would like to thank the RIEGL Agency (Five-star Electronic Technology Company Limited) who provided the instrument Rieg1 VZ-400i.

## REFERENCES

- [1] J. Selbeck, V. Dworak, and D. Ehlert, "Testing a vehicle-based scanning LiDAR sensor for crop detection," *Can. J. Remote Sens.*, vol. 36, no. 1, pp. 24–35, Jan. 2010.
- [2] J. Lumme *et al.*, "Terrestrial laser scanning of agricultural crops," *Int. J. Remote Sens.*, vol. 26, no. 7, pp. 563–566, Jul. 2008.
- [3] D. J. Mulla, "Twenty five years of remote sensing in precision agriculture: Key advances and remaining knowledge gaps," *Biosyst. Eng.*, vol. 114, no. 4, pp. 358–371, Apr. 2013.
- [4] T. Jarmer, "Spectroscopy and hyperspectral imagery for monitoring summer barley," *Int. J. Remote Sens.*, vol. 34, no. 17, pp. 6067–6078, Sep. 2013.
- [5] J. Romeo *et al.*, "Camera sensor arrangement for crop/weed detection accuracy in agronomic images," *Sensors*, vol. 13, no. 4, pp. 4348–4366, 2013.
- [6] W. Wagner, M. Hollaus, C. Briese, and V. Ducic, "3D vegetation mapping using small-footprint full-waveform airborne laser scanners," *Int. J. Remote Sens.*, vol. 29, no. 5, pp. 1433–1452, Mar. 2008.
- [7] M. Friedli, N. Kirchgessner, C. Grieder, F. Liebisch, M. Mannale, and A. Walter, "Terrestrial 3D laser scanning to track the increase in canopy height of both monocot and dicot crop species under field conditions," *Plant Methods*, vol. 12, no. 1, p. 9, Dec. 2016.
- [8] J. Llorens, E. Gil, J. Llop, and M. Queraltó, "Georeferenced LiDAR 3D vine plantation map generation," *Sensors*, vol. 11, no. 6, pp. 6237–6256, Jun. 2011.
- [9] A. K. Moorthy, C.-C. Su, A. Mittal, and A. C. Bovik, "Subjective evaluation of stereoscopic image quality," *Signal Process. Image Commun.*, vol. 28, no. 8, pp. 870–883, Sep. 2013.
- [10] K. Koenig, B. Höfle, M. Hämmeler, T. Jarmer, B. Siegmann, and H. Lilienthal, "Comparative classification analysis of post-harvest growth detection from terrestrial LiDAR point clouds in precision agriculture," *J. Photogramm. Remote Sens.*, vol. 104, pp. 112–125, Jun. 2015.
- [11] J. U. H. Eitel, T. S. Magney, L. A. Vierling, and G. Dittmar, "Assessment of crop foliar nitrogen using a novel dual-wavelength laser system and implications for conducting laser-based plant physiology," *J. Photogramm. Remote Sens.*, vol. 97, pp. 229–240, Nov. 2014.
- [12] X. Zhu *et al.*, "Foliar and woody materials discriminated using terrestrial LiDAR in a mixed natural forest," *Int. J. Appl. Earth Observ. Geoinform.*, vol. 64, pp. 43–50, Feb. 2018.
- [13] A. Kashani, M. Olsen, C. Parrish, and N. Wilson, "A review of LiDAR radiometric processing: From ad hoc intensity correction to rigorous radiometric calibration," *Sensors*, vol. 15, no. 11, pp. 28099–28128, Nov. 2015.
- [14] B. Jutzi, and H. Gross, "Normalization of LiDAR intensity data based on range and surface incidence angle," *Int. Arch. Photogramm. Remote Sens. Spat. Inf. Sci.*, vol. 38, pp. 213–218, Sep. 2009.
- [15] T. Xu, L. Xu, B. Yang, X. Li, and J. Yao, "Terrestrial laser scanning intensity correction by piecewise fitting and overlap-driven adjustment," *Remote Sens.*, vol. 9, no. 11, p. 1090, Oct. 2017.
- [16] S. Kaasalainen *et al.*, "Brightness measurements and calibration with airborne and terrestrial laser scanners," *IEEE Trans. Geosci. Remote Sens.*, vol. 46, no. 2, pp. 528–534, Feb. 2008.
- [17] W. Fang, X. Huang, F. Zhang, and D. Li, "Intensity correction of terrestrial laser scanning data by estimating laser transmission function," *IEEE Trans. Geosci. Remote Sens.*, vol. 53, no. 2, pp. 942–951, Feb. 2015.
- [18] M. Pfennigbauer and A. Ullrich, "Improving quality of laser scanning data acquisition through calibrated amplitude and pulse deviation measurement," *Proc. SPIE*, vol. 29, p. 7684, Apr. 2010.
- [19] L. Breiman, "Random forests," *Mach. Learn.*, vol. 45, no. 1, pp. 5–32, 2001.
- [20] M. Belgiu and L. Drăguț, "Random forest in remote sensing: A review of applications and future directions," *J. Photogramm. Remote Sens.*, vol. 114, pp. 24–31, Apr. 2016.
- [21] Y. Shao, J. B. Campbell, G. N. Taff, and B. Zheng, "An analysis of cropland mask choice and ancillary data for annual corn yield forecasting using MODIS data," *Int. J. Appl. Earth Observ. Geoinf.*, vol. 38, pp. 78–87, Jun. 2015.
- [22] E. M. Abdel-Rahman, O. Mutanga, E. Adam, and R. Ismail, "Detecting *Sirex noctilio* grey-attacked and lightning-struck pine trees using airborne hyperspectral data, random forest and support vector machines classifiers," *J. Photogramm. Remote Sens.*, vol. 88, pp. 48–59, Feb. 2014.
- [23] RIEGL Laser Measurement Systems GmbH, Austria. Datasheet RIEGL VZ-400i. Accessed: Apr. 26, 2018. [Online]. Available: [http://www.riegl.com/uploads/ttx\\_pxpriegldownloads/RIEGL\\_VZ-400i\\_Datasheet\\_2017-12-18.pdf](http://www.riegl.com/uploads/ttx_pxpriegldownloads/RIEGL_VZ-400i_Datasheet_2017-12-18.pdf)
- [24] Girardeau-Montaut, D. Cloudcompare. A 3D Point Cloud and Mesh Processing Free Software. Accessed: Jun. 21, 2018. [Online]. Available: [www.danielgm.net/cc](http://www.danielgm.net/cc)